

Lateral input-optic displacement in a diffractive Fabry-Perot cavity

J. Hallam¹, S. Chelkowski¹, A. Freise¹, B.W. Barr², S. Hild²,
K.A. Strain², O. Burmeister³ and R. Schnabel³

¹ School of Physics and Astronomy, University of Birmingham, Edgbaston, Birmingham B15 2TT, United Kingdom

² Institute for Gravitational Research, Department of Physics and Astronomy, University of Glasgow, Glasgow, G12 8QQ, United Kingdom

³ Max-Planck-Institut für Gravitationsphysik (Albert-Einstein-Institut) and Leibniz Universität Hannover, Callinstr. 38, D-30167 Hannover, Germany.

E-mail: jmh@star.sr.bham.ac.uk

Abstract. All-reflective configurations have been suggested for future laser-interferometric gravitational wave detectors. Diffraction gratings would be required as core elements of any such design. In this paper, coupling of lateral grating displacement to the output ports of a diffractive Fabry-Perot cavity was derived using a steady-state technique. The signal to noise ratio versus a potential gravitational wave signal was compared for each cavity output port. For a cavity featuring parameters similar to the planned Advanced Virgo instrument, we found the forward-reflected port offers the highest SNR at low frequencies. Furthermore, the lateral isolation suspension requirements were relaxed by a factor of twenty at a frequency of 10 Hz versus the transmitted port.

1. Introduction

The sensitivity of proposed gravitational wave detectors utilising the laser-interferometric technique might be improved by reducing the number of transmissive optical components and at the extreme adopting an all-reflective optical configuration [1]. Particular focus falls on the beam-splitter and cavity input mirrors of a Michelson interferometer with Fabry-Perot arm cavities as are used in LIGO [2] and Virgo [3] and which will be used for the upgrades to those detectors.

It is expected that an all-reflective configuration will eliminate transmissive thermal noises and free optical substrates to be opaque. This would widen the range of materials that could be chosen allowing the selection of other desirable properties. Further, proposals to reduce the shot noise contribution by increasing laser power are likely to introduce technical problems such as thermal lensing which are only significant with transmissive optics.

Diffraction gratings are the only possible replacements for the cavity input mirrors and beam-splitters that would still allow an all-reflective interferometer to function in a Michelson-esque way [4]. Herein we consider the case where a diffraction grating is used in place of a Fabry-Perot cavity input mirror [5].

Prior work has found that state of the art gratings cannot achieve diffraction efficiencies approaching the reflection efficiencies available from multilayer dielectric coatings [6, 7]. Thus

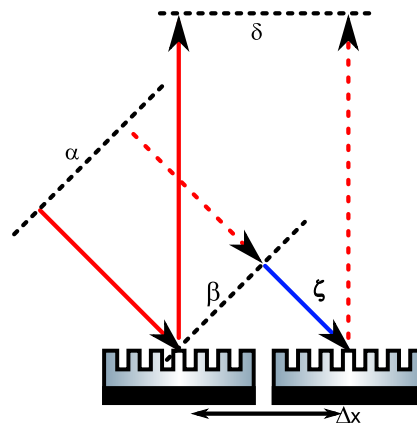


Figure 1. Wavefronts coupling through a diffraction grating. The wavefront (propagation vector shown in solid red) originates at α , continues to β and is diffracted to δ . Displacing the grating by a lateral distance of Δx , causes the wavefront (propagation vector shown red-dashed) to pass through the additional path length ζ (propagation vector shown in solid blue).

the high-finesse Fabry-Perot cavities required for gravitational wave detection cannot be formed by recoupling the diffracted light back into the cavity; rather, a diffraction grating with low diffraction efficiency must be used with the diffractive order serving as the incoupler (equivalent to a conventional cavity's input mirror transmissivity). In the case of a three-port, second-order-Littrow configured cavity (as shown in Figure 2) the finesse is determined by the zeroth-order diffraction efficiency (sometimes called reflection efficiency) of the grating, which can be made equivalent to a conventional mirror reflectivity using the same multilayer coating techniques.

2. Lateral grating displacement phase noise

By contrast to a standard Fabry-Perot cavity using a transmissive input mirror the geometry enforced by the use of a diffraction grating causes additional coupling of grating displacement into phase noise [8].

This phase noise stems purely from the geometry of the optics and hence the grating equation alone suffices to calculate it, so long as the geometry of the set-up is known. The phase change resulting from the displacement is due to a path-length difference ζ between parallel wavefronts, shown for a simple geometrical case in Figure 1.

This noise occurs due to displacement across the grating's corrugation with respect to the beam. Such displacement can appear from angular misalignment of the end-mirror projecting the beam across the grating, or the misalignment of the injection optics causing a similar effect, or physical displacement of the grating itself. Freise et al determined that, by assuming a sensitivity goal of $h = 10^{-23}/\sqrt{\text{Hz}}$, using a set of parameters reasonably consistent with Virgo [3] and a grating both typical and practical, a standard cavity required angular end mirror alignment of $\gamma < 2 \cdot 10^{-16} \text{ rad}/\sqrt{\text{Hz}}$ whereas a three-port coupled grating cavity required $\gamma < 1 \cdot 10^{-21} \text{ rad}/\sqrt{\text{Hz}}$. Hence five orders of magnitude improvement in the end turning mirror alignment is required for equivalent insensitivity to this noise source. In this article we consider the physical displacement of the grating which couples into phase noise.

3. Frequency domain model of phase noise coupling in a grating cavity

In order to analyse the coupling of the phase noise introduced by grating displacement to the output ports of a grating cavity quantitatively we performed a frequency domain analysis. By

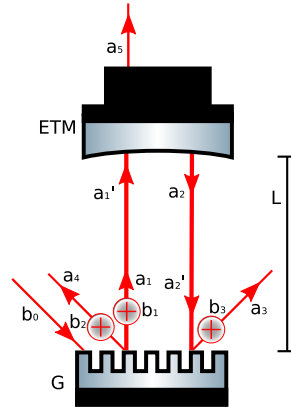


Figure 2. External input port b_0 , internal input ports b_1 , b_2 , b_3 (marked by encircled addition symbols) and the transfer ports a_1 , a_1' , a_2 and a_2' in a grating cavity

carrying out this analysis for the effect of a potential gravitational-wave signal and the noise effect of lateral grating displacement we obtained the signal to noise ratio (SNR) at all three output ports of the grating cavity. Particularly important was to find the port with the highest SNR, a potentially strong driver on how to integrate such a cavity into interferometer configurations.

To compare the signal to noise ratio at the different output ports we performed the mathematical steps outlined here and discussed fully elsewhere [9]. First we determined the grating coupling relations using the symmetrical coupling matrices previously determined in [10]. Using these coupling relations we calculated both carrier light fields (shown blue in Figure 3) incident on the grating in terms of a single external input carrier light field. By definition, these carrier fields were unchanged in frequency from the input light field and therefore contained neither gravitational wave signal nor grating displacement noise.

These were then used to determine the amplitude of the sideband fields at the location of their creation. The sidebands were created by modulation, either from a gravitational wave or grating displacement. Again using the coupling relations we propagated these sidebands to the output ports and obtained their amplitude. Dividing the gravitational wave sidebands by the grating displacement noise sidebands obtained the signal to noise ratio.

3.1. Lateral grating displacement noise coupling in a grating cavity

The complex amplitudes a_3 , a_4 and a_5 associated with the upper noise sideband at each output consistent with Figure 2 are given by:

$$a_3 = ip_0\eta_1^2 e^{-2i\phi_1} \frac{\pi\Delta x}{d} (B_u - B_c), \quad (1)$$

$$a_4 = ip_0\eta_1^2 e^{-2i\phi_1} \frac{\pi\Delta x}{d} (B_u + B_c) + ip_0\eta_2 e^{-i\phi_2} \frac{2\pi\Delta x}{d}, \quad (2)$$

$$a_5 = -p_0\eta_1 e^{-i\phi_1} \frac{\pi\Delta x}{d} \frac{B_u}{\rho_2 e^{-ik_u L} \tau_2}. \quad (3)$$

Where p_0 is the complex amplitude for the carrier field input in the port b_0 , ρ_2 is the reflectivity of the end-mirror, ρ_0 is the reflectivity of the diffraction grating in the special case of zeroth order diffraction normal to the surface of the grating, η_1 and η_2 are the first and second order diffraction efficiencies and ϕ_1 and ϕ_2 are the phase shifts associated with them, d is the periodicity of the grating, L is the cavity length and Δx is the displacement of the grating. $B_c = D(\omega_c)\rho_2 e^{-2ik_c L}$

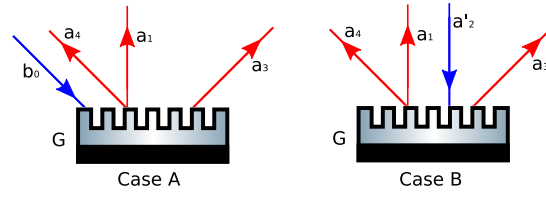


Figure 3. Input (b_0 , a'_2 , shown blue) and output (a_1 , a_3 , a_4 , shown red) light field amplitudes at a phase modulating grating in second-order Littrow-configuration in case A, and zeroth-order-Littrow configuration in case B (labels consistent with Figure 2).

with $D(\omega_c) = 1/(1 - \rho_2\rho_0e^{-2ik_cL})$, where ω_c is the absolute frequency of the input carrier light field and k_c is the wavevector ($2\pi/\lambda$) associated with it. B_u can be similarly expressed except for its own absolute frequency given by $\omega_u = \omega_c + \omega_m$, the carrier frequency plus the frequency with which the grating is displaced. A similar result could be obtained for the lower sideband by subtracting rather than adding the modulation frequency, notationally replacing ‘ u ’ with ‘ l ’ in the subscript. Thus we computed the optical signal in all output ports generated by lateral motion of the grating.

3.2. Signal coupling in a grating cavity

The complex amplitudes a_3 , a_4 and a_5 associated with the upper signal sideband induced by potential gravitational wave at each output consistent with Figure 2 are given by:

$$a_3 = ip_0\eta_1^2 e^{-2i\phi_1} \frac{2\pi\Delta z}{\lambda} B_c B_u, \quad (4)$$

$$a_4 = ip_0\eta_1^2 e^{-2i\phi_1} \frac{2\pi\Delta z}{\lambda} B_c B_u, \quad (5)$$

$$a_5 = -p_0\eta_1 e^{-i\phi_1} \frac{2\pi\Delta z}{\lambda} \frac{B_c}{\rho_2 e^{-ik_c L}} \frac{B_u}{\rho_2 e^{-ik_u L}} \tau_2. \quad (6)$$

Where B_c and B_u retain their prior meanings, excepting that ω_m will now be the frequency of mirror motion induced by the gravitational wave. The gravitational wave was assumed to propagate perpendicular to the cavity, and it’s effect has been expressed in terms of an displacement of the mirror Δz equivalent to our previously considered grating displacement, resulting in modulation index $m = 4\pi\Delta z/\lambda$. This effect appears at cavity internal input b_1 in Figure 2. Thus we computed the optical signal in all output ports due to a potential gravitational wave signal.

4. Ratio of signal to noise at grating cavity output ports

An appropriate figure of merit to evaluate the length-sensing performance of the different grating cavity output ports is the ratio of gravitational wave signal to lateral grating displacement noise (the signal to noise ratio). The SNR was derived by dividing the absolute field amplitude in the gravitational wave case by the absolute field amplitude in the grating lateral displacement case for each output. For a standard two-mirror cavity with equivalent finesse the SNR will be infinity as in principle two-mirror cavity input mirrors are insensitive to lateral displacement although in practice any suspension system has some coupling from lateral excitation to longitudinal displacement. Using Equations 1 through 3 and 4 through 6 we obtained the following signal to noise ratios at the output port of the equivalent subscript:

$$\text{SNR}_3 = \Lambda_{\text{cav}} \frac{B_u}{B_u - B_c}, \quad (7)$$

$$\text{SNR}_4 = \Lambda_{\text{cav}} \frac{B_u}{B_u + B_c + 2\eta_2/\eta_1^2 e^{-i\phi_2+2i\phi_1}}, \quad (8)$$

$$\text{SNR}_5 = \Lambda_{\text{cav}}/\rho_2 e^{-ik_c L}, \quad (9)$$

with

$$\Lambda_{\text{cav}} = \frac{2d\Delta z B_c}{\lambda \Delta x}. \quad (10)$$

These equations reveal the differences between the ratio of gravitational wave signal to lateral grating displacement noise for the three cavity output ports. The SNR at the back-reflected (a_3) and forward-reflected (a_4) output ports contain the modulation frequency dependent term B_u whilst at the transmitted (a_5) port the SNR is independent of the frequency of modulation. This frequency independence is somewhat counter-intuitive and only occurs because the displacement-noise and gravitational wave signal were compared at the same frequency. As can be seen from Equations 3 and 4 the transmitted output port has the same frequency response to both signal and noise.

It was found that the SNR for the forward-reflected (a_4) and back-reflected (a_3) output ports includes the SNR from inside the cavity Λ_{cav} , multiplied by a fraction containing the different resonance factors for the carrier light field and the sidebands. The η_2/η_1^2 term in Equation 8 will be small despite the square in the denominator, as the η_2 diffraction efficiency is a loss term for this configuration and will be minimised by design, whereas η_1 is the much larger input coupling efficiency term. Apart from this term the only difference between Equations 7 and 8 is whether the resonance terms of the carrier and sideband in the denominator are added or subtracted. The important feature of these equations is that $B_u \approx B_c$ for modulation frequencies within the cavity bandwidth. This brings the denominator in Equation 7 close to zero, thus strongly increasing the SNR at the forward-reflected (a_3) port. There is therefore a partial cancellation of the phase noise introduced from lateral grating displacement at the forward-reflected port.

Physically this can be understood quite simply: The carrier light field enters the cavity, generating noise sidebands proportional to its intensity. It then resonates in the cavity and increases in intensity proportional to the cavity finesse. When it exits the cavity via the grating it generates noise sidebands proportional to its new, increased intensity. The input sidebands generated when the carrier entered the cavity will partially cancel with these output sidebands. The cancellation will be complete if the input sidebands also increased in intensity due to resonance in the cavity. How resonant these input sidebands are within the cavity depends on the finesse which sets the cavity's bandwidth and on how far they are from the perfect resonant frequency of the cavity (defined by the carrier frequency). Therefore we can say that the cancellation will be quite good for modulation frequencies within the cavity bandwidth.

From this it is clear that of the three expected sources of displacement noise: angular end-mirror misalignment, injection optic misalignment and lateral grating displacement only the latter two will benefit from this cancellation, as only they will generate both input and output sidebands. The end-mirror misalignment occurs within the cavity and hence generates only output sidebands. It might appear that misaligned injection pointing only generates input sidebands, but it has been shown that this also changes the alignment of the field circulating in the cavity [11] and hence also generates output sidebands. The end-mirror angular misalignment will remain a problem [8]; however, the large number of optical elements in the injection path, and that many of them are not suspended suggests the reduction of noise from this source will

be important. In any-case suspension design will be eased if the transverse isolation requirement imposed by the grating can be weakened.

It is also necessary to discuss where the gravitational wave signal appears most strongly as given by Equations 1 through 6. It is useless to have good SNR versus the displacement noise source if the signal is not strongly present. For proposed interferometric gravitational wave detector layouts the end-mirror will be highly reflective (ρ_2 will be close to one) and therefore the complex field amplitudes for the potential gravitational wave signal will obey the relations $a_3 \gg a_5$, $a_4 \gg a_5$. There will be approximately half the signal in the forward-reflected port with good SNR, half will be in the back-reflected port with poor SNR and very little will be in the transmitted port.

In a broader context this result demonstrates that there is a small but useful advantage to be gained by utilising the forward-reflected output port of a three-port-coupled diffractive cavity for detection, especially to the exclusion of the back-reflected port if at all possible, although this will result in the loss of some signal. Due to the small amount of gravitational wave signal present there, the dumping of the transmitted port will have negligible effect, advantageous as many configurations will place this port at an end-station some kilometers from the central optics. In any-case it is likely this lost light can be used for monitoring purposes, e.g. in alignment control.

Conversely as both forward-reflected and back-reflected output ports will be co-located, and likely co-located at the central optics for both arm-cavities if a Michelson-like design is used it may be preferred to use both outputs, or to link the two cavities in some way. Such an idea was sketched by Drever [4] although we are aware of no formal noise-analysis of such a configuration, which anyway could not be complete with respect to noise without the work presented above and previously in [9].

4.1. Numerical result

In this section we present a quantitative analysis for one example configuration of a three-port-coupled diffractive cavity. The figures selected were $L = 3$ km, $\rho_2 = \sqrt{0.99995}$ (50 ppm power transmittance) and $\rho_0 = \sqrt{0.95}$ for a possible implementation of diffractive cavities in an Advanced Virgo-like interferometer [12]. Demanding that the $\mu = 1$ diffraction order serves as the input coupler imposes the grating design requirement $d \leq 2\lambda$ [13]. Grating phase relations impose the minimum possible value of $\eta_2 \geq 0.0127$. From [10] for minimum η_2 we find that $\eta_2 e^{-i\phi_2} = -0.0127$, and the cavity input parameters set $\eta_1 e^{-i\phi_1}$. Together these fix the last term in the denominator in Equation 8, and as expected it was found to be small compared to the other terms of the denominator. Setting the carrier light resonant in the cavity imposes $e^{-2ik_c L} = 1$ and the modulation frequency ω_m of the lateral grating displacement is chosen to be 10 Hz.

Our interest focuses on the relative magnitude of the frequency sidebands. As in Freise et al [8] we set $\Delta z/\Delta x = 1$ in order to compare potential gravitational-wave signal to the effect of grating displacement. Since we are dealing with complex field amplitudes for this analysis we take the absolute value of the ratios. The ratio contains a real part as well as an imaginary part, so we assumed that the a homodyne measurement can be performed, choosing the readout quadrature of each output port individually by adding the proper local oscillator. This yields the following result:

$$|\text{SNR}_3| = 3181, \quad (11)$$

$$|\text{SNR}_4| = 79, \quad (12)$$

$$|\text{SNR}_5| = 158. \quad (13)$$

In all output ports the SNR is greater than one, as the cavity naturally suppresses the displaced grating phase noise sidebands versus the signal sidebands by a factor of 158 as seen

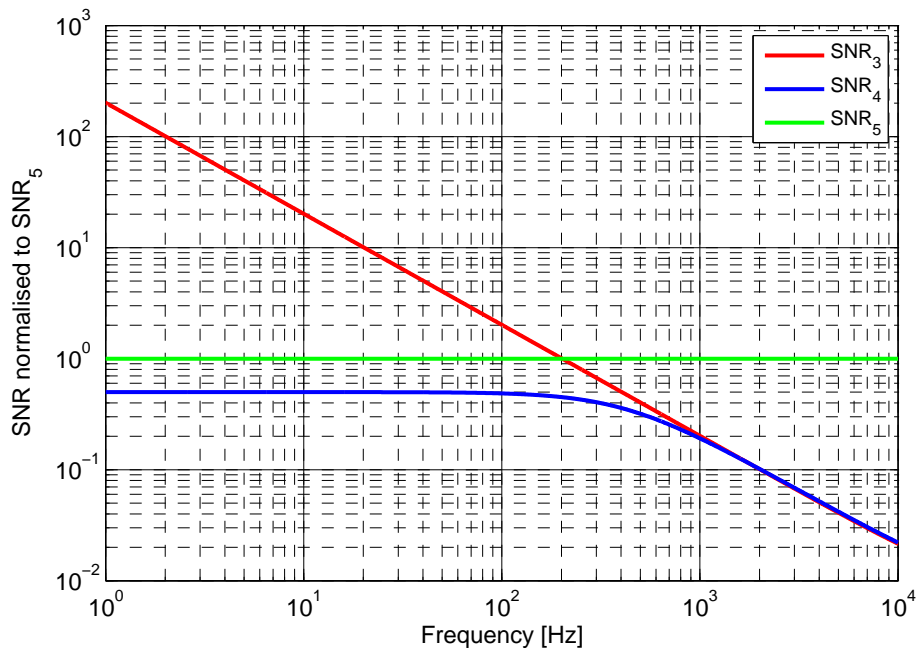


Figure 4. Signal to noise ratio of gravitational wave equivalent mirror displacement and lateral grating displacement at the three different output ports of a grating gravity. All traces are normalized to SNR_5 .

in the transmitted output port. This is because the displacement noise only appears when light enters the cavity, whereas the gravitational wave signal appears in every round trip. In the three-port-coupled case we have found a further factor of twenty improvement in the SNR can be obtained through the cancellation of input and output grating displacement sidebands in the forward-reflected (a_3) port compared to the transmitted (a_5) port.

In a next step, instead of a single frequency of interest, we consider modulation frequencies covering the full detection band of gravitational wave detectors. As SNR_3 and SNR_4 are frequency dependent, we normalise them to SNR_5 and plot them over frequency to obtain Figure 4.

At low modulation frequencies where the sidebands are to a good approximation resonant in the cavity, imposing $B_u \approx B_c$ the forward-reflected port (a_3) has good cancellation between the input and output sidebands generated by the grating lateral displacement. This results in high SNR compared to the transmitted port (a_5). In the back-reflected port (a_4) summation occurs instead of cancellation and hence the SNR is lower than in the transmitted port. As the modulation frequency diverges from the cavity resonance, the sidebands do not resonate in either the gravitational-wave or grating lateral displacement case as B_u trends to zero. Thus the sideband contribution generated when the carrier field exits the cavity (the B_c terms in the denominator of Equations 7 and 8) dominates causing the SNR of the reflected ports to converge below the level of the transmitted port.

4.2. Suspension requirements

The potential suspension requirements for a grating cavity used as an arm cavity within the planned Advanced Virgo detector provide a useful reference point for this work. Using a contemporary Advanced Virgo design sensitivity [14] we plot in Figure 5 the corresponding tolerable lateral grating motion for each of the three potential readout ports of the grating arm

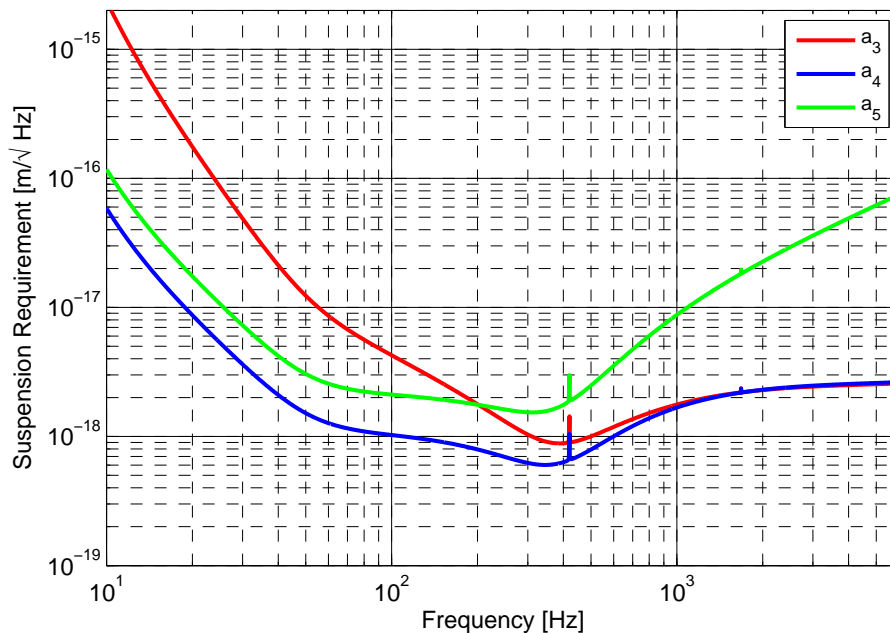


Figure 5. Suspension requirement for the maximum tolerable lateral grating displacement that is necessary to achieve the Advanced Virgo design sensitivity. The suspension required strongly depends on the readout port as well as the frequency of interest. At low frequencies the phase noise suppression in port a_3 allows significant relaxation of the required suspension isolation. The narrow peak around 410 Hz is due to a resonance in the Advanced Virgo design, not a grating effect.

cavity.

We have found that we can relax by a factor of twenty at 10 Hz (Figure 5) the suspension requirement for the the un-suppressed transmitted (a_5) port by utilizing the forward-reflected (a_3) port for the signal readout. As discussed above this suppression, because it relies on cancellation between input and output noise sidebands, only applies to the suspension of the diffractive optic itself (shown in Figure 5) and proportionally to the injection optics pointing. It does not, unfortunately, reduce the end-mirror alignment requirements calculated by Freise et al [8].

5. Summary and Outlook

Diffraction gratings are an important avenue of research because they allow all-reflective interferometer configurations. Apart from offering thermal noise improvements which may be especially relevant in mitigating effects made important when high power is used to reduce shot-noise contribution, these diffraction gratings may allow new configurations which have other advantageous properties without significantly changing the overall detector shape.

An additional noise source is lateral grating displacement relative to the beam causing path-length differences that couple phase-noise into the gravitational wave detection channel. From [8] the grating-cavity end-mirror angular alignment suspension requirement (five orders of magnitude higher than that required by a two-mirror cavity), and associated likely increases in injection optic pointing and lateral grating stability were a significant impetus against using grating cavities.

To determine the effect a frequency domain analysis was carried out to calculate the coupling

of lateral grating displacement to the different output ports of a three-port-coupled grating cavity [9]. For the output port in forward-reflection of the grating we found a suppression of phase noise originating from lateral grating displacement over the transmitted port, resulting in a factor of twenty relaxation in the lateral displacement suspension requirement at 10 Hz. This will likely also apply to the injection optics pointing stability. This factor will increase with a wide cavity bandwidth and hence the noise suppression will be greater in cavities of lower finesse.

Acknowledgments

This work was supported by the Science and Technology Facilities Council (STFC), the European Gravitational Observatory (EGO) and the Deutsche Forschungsgemeinschaft (DFG) within the Sonderforschungsbereich (SFB) TR7.

References

- [1] K. X. Sun and R. L. Byer. All-reflective Michelson, Sagnac, and Fabry-Perot interferometers based on grating beam splitters. *Optics letters*, 23(8):567–569, April 1998.
- [2] J. R. Smith and LIGO Scientific Collaboration. The path to the enhanced and advanced LIGO gravitational-wave detectors. *Classical and Quantum Gravity*, 26(11):114013–+, June 2009.
- [3] F. Acernese et al. Virgo status. *Classical and Quantum Gravity*, 25(18):184001 (9pp), 2008.
- [4] R. W. P. Drever. Concepts for Extending the Ultimate Sensitivity of Interferometric Gravitational Wave Detectors Using Non-transmissive Optics with Diffractive or Holographic Coupling. In *Proceedings of the Seventh Marcel Grossman Meeting on recent developments in theoretical and experimental general relativity, gravitation, and relativistic field theories*, pages 1401–+, 1996.
- [5] A. Bunkowski, O. Burmeister, P. Beyersdorf, K. Danzmann, R. Schnabel, T. Clausnitzer, E.-B. Kley, and A. Tünnermann. Low-loss grating for coupling to a high-finesse cavity. *Optics Letters*, 29:2342–2344, October 2004.
- [6] A. Bunkowski, O. Burmeister, T. Clausnitzer, E.-B. Kley, A. Tünnermann, K. Danzmann, and R. Schnabel. Optical characterization of ultrahigh diffraction efficiency gratings. *Applied Optics*, 45:5795–5799, August 2006.
- [7] M. D. Perry, R. D. Boyd, J. A. Britten, D. Decker, B. W. Shore, C. Shannon, and E. Shults. High-efficiency multilayer dielectric diffraction gratings. *Optics Letters*, 20:940–942, April 1995.
- [8] A. Freise, A. Bunkowski, and R. Schnabel. Phase and alignment noise in grating interferometers. *New Journal of Physics*, 9:433–+, December 2007.
- [9] J. Hallam, S. Chelkowski, A. Freise, S. Hild, B. Barr, K. A. Strain, O. Burmeister, and R. Schnabel. Coupling of lateral grating displacement to the output ports of a diffractive FabryPerot cavity. *Journal of Optics A: Pure and Applied Optics*, 11(8):085502–+, August 2009.
- [10] A. Bunkowski, O. Burmeister, K. Danzmann, and R. Schnabel. Input-output relations for a three-port grating coupled fabry-perot cavity. *Opt. Lett.*, 30:1183–1185, 2005.
- [11] E. Morrison, D. I. Robertson, H. Ward, and B. J. Meers. Experimental demonstration of an automatic alignment system for optical interferometers. *Appl. Opt.*, 33:5037–5040, August 1994.
- [12] The Virgo Collaboration. Advanced virgo baseline design. Technical report, Virgo, 2009.
- [13] T. Clausnitzer, E.-B. Kley, A. Tünnermann, A. Bunkowski, O. Burmeister, K. Danzmann, R. Schnabel, S. Gliech, and A. Duparré. Ultra low-loss low-efficiency diffraction gratings. *Optics Express*, vol. 13, Issue 12, p.4370, 13:4370–+, June 2005.
- [14] S Hild, G Losurdo, and A Freise. Sensitivity options for the advanced virgo preliminary design. Technical report, Virgo, 2009.